Infrared Cavity-Enhanced Colloidal Quantum Dot Photovoltaics Employing Asymmetric Multilayer Electrodes

Se-Woong Baek,[†,‡] Olivier Ouellette,[†] Jea Woong Jo,[†] Jongmin Choi,[†] Ki-Won Seo,[‡] Junghwan Kim,[†] Bin Sun,[†] Sang-Hoon Lee,[‡] Min-Jae Choi,[†] Dae-Hyun Nam,[†] Li Na Quan,[†] Juhoon Kang,[‡] Sjoerd Hoogland,[†] F. Pelayo García de Arquer,[†] Jung-Yong Lee,*[,‡] and Edward. H Sargent*[,†]

†Department of Electrical and Computer Engineering, University of Toronto, 10 King's College Road, Toronto, Ontario M5S 3G4, Canada

‡Graduate School of Energy, Environment, Water, and Sustainability (EEWS), Korea Advanced Institute of Science and Technology (KAIST), Daejeon 34141, Republic of Korea

Ⓢ *Supporting Information*

ABSTRACT: Efficient infrared (IR) optoelectronic devices, crucial for emerging sensing applications and also for solar energy harvesting, demand high-conductivity IR-transparent electrodes. Here we present a new strategy, one based on oxide/metal/oxide multilayers, that enables highly transparent IR electrodes. Symmetry breaking in the oxide stack leads to broad and high transmittance from visible to IR wavelengths, while a low refractive index doped oxide as a front layer boosts IR transmittance. The combination of doped oxide and ultrathin metal film allows for low sheet resistance while maintaining IR transparency. We engineer the IR microcavity effect using the asymmetric multilayer approach to tailor the distribution of incident radiation to maximize IR absorption in the colloidal quantum dot (CQD) layer. As a result, the absorption-enhanced IR CQD solar cells exhibit a photoelectric conversion efficiency of 70% at a wavelength of 1.25 μm, i.e., well within the spectral range in which silicon is blind.
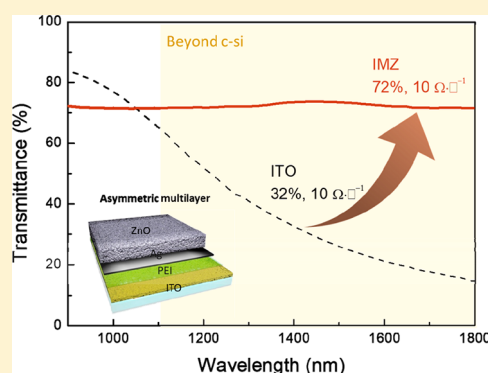
Photoelectric conversion of infrared (IR) radiation is key for sensing applications in surveillance, medicine, and communications;[1] in emerging fields such as machine vision and gesture recognition; and for full-spectrum solar energy harvesting (Figure 1).

Solution-processed materials such as CQDs combine facile and scalable manufacturing with spectral tunability and are particularly suited for these applications.[2] The absorption coefficient of IR-absorbing lead chalcogenides, on the order of 10^4 cm^{-1} at the exciton peak, demands CQD films thicker than 1 μm to absorb IR light fully. The diffusion length in CQD solids (the distance over which photogenerated charges can diffuse before they recombine) is limited today to approximately hundreds of nm, leading to a present-day compromise between light absorption and photocarrier extraction.

Light management strategies that increase CQD absorption in the IR for a given thickness are therefore of high importance.[3] This is especially challenging in the IR, where widely employed transparent conductive electrodes (TCEs) such as indium tin oxide (ITO) and fluorine tin oxide (FTO) exhibit increased free-carrier absorption and lead directly to substantially reduced optical transmittance.[4]

The design of TCEs that are highly conductive, exhibit high IR transmittance, and allow implementation of IR light-trapping strategies enables therefore the realization of more efficient sensors and photovoltaic technologies. Although a variety of innovative TCEs have been studied as ITO alternatives, including carbon derivatives,[5] oxide/metal/oxide (OMO) multilayers,[6−9] and metal meshes[10] and grids,[11] these have typically been focused on visible performance and its applications. Their designs have been aimed at minimizing UV losses from oxide band-to-band absorption and visible parasitic absorption in the metal layers.

In this study, we present a strategy instead aimed at maximizing IR transmittance and conductivity jointly, and we do this using a newly designed asymmetric oxide/metal/oxide architecture. Our approach provides a high average IR
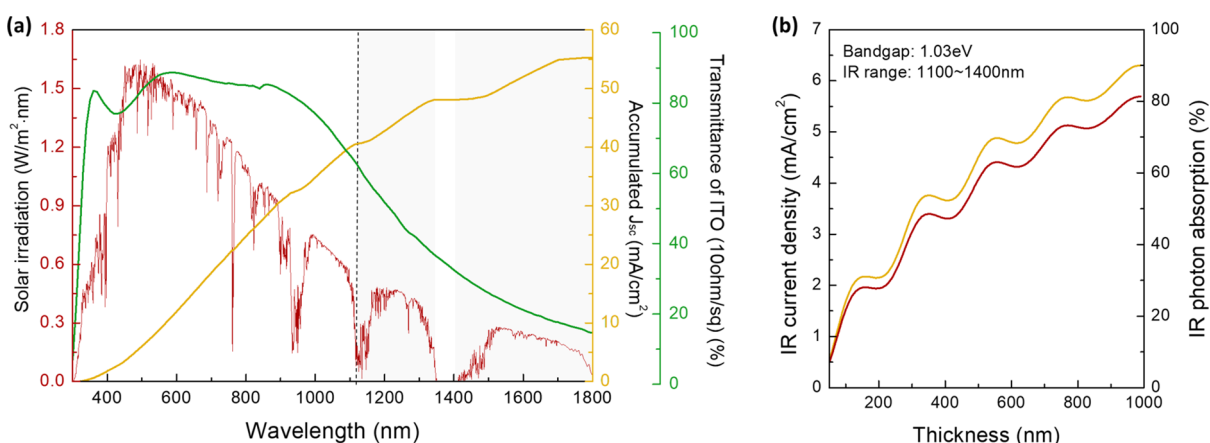
Figure 1. (a) AM1.5G solar irradiation (red); available cumulative current density (yellow); optical transmittance of an ITO transparent electrode with a sheet resistance of 10 ohm/□ (green). The gray area depicts the IR wavelength range from which extra photocurrent can be extracted beyond cSi. (b) Optical calculation results of IR current density (yellow) and IR photon absorption (red) of CQD solar cells as a function of CQD layer thickness.
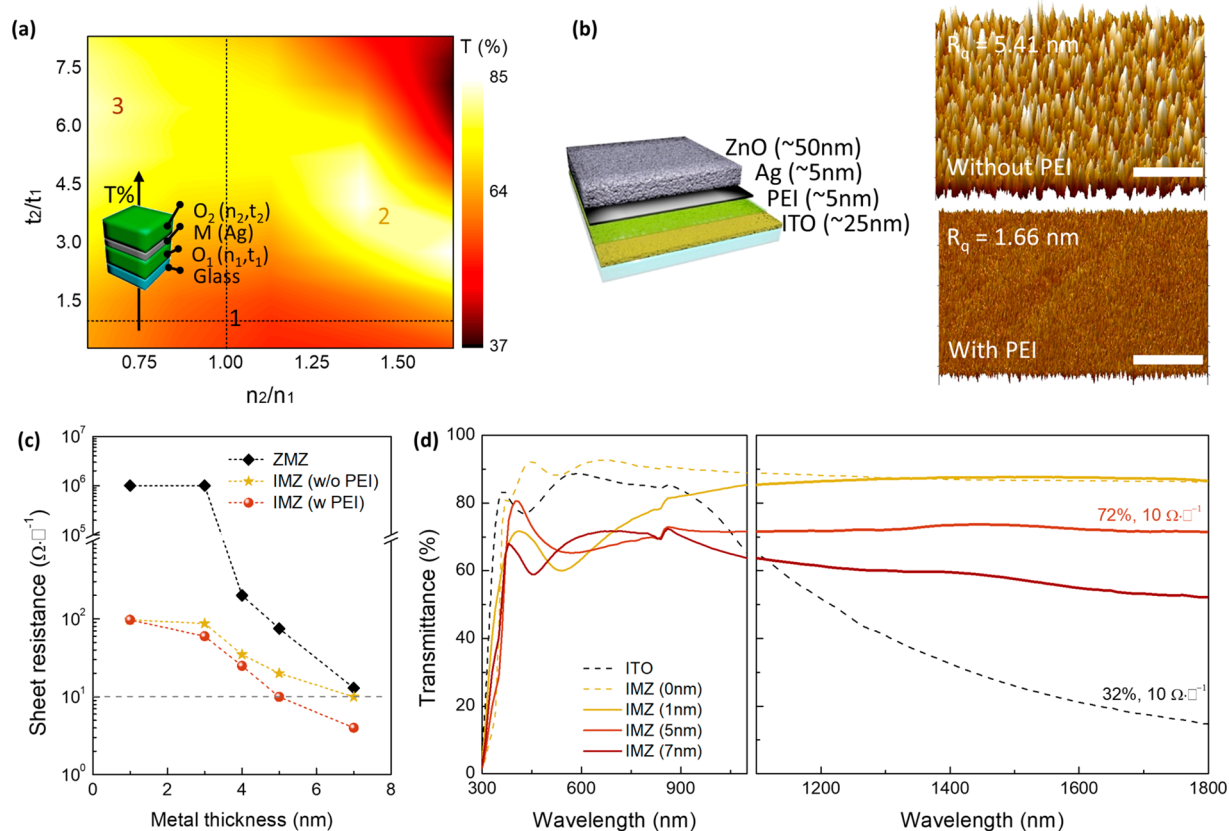

Figure 2. (a) IR transmittance as a function of the thickness and refractive index ratio of oxide (t_1, n_1)/metal(5 nm)/oxide(t_2, n_2). (b) Schematic illustration of the IMZ structure and 3D AFM topography image of a Ag film on an ITO substrate without and with a PEI seed layer. Scale bar: 500 nm. (c) Sheet resistance of ZnO(30 nm)/Ag/ZnO(50 nm) (black), ITO(25 nm)/Ag/ZnO(50 nm) (yellow), and ITO:PEI/Ag/ZnO (red) as a function of Ag thickness. (d) Optical transmittance of conventional thick ITO (10 Ω/□, 155 nm) (black dashes) and IMZ with various Ag thicknesses.

transmittance (AIRT) across the broad spectral range of 1100−1800 nm. Its performance represents a fully 2.3-fold improvement in AIRT (%) compared to conventional ITO for the same sheet resistance of 10 Ω/□. The new architecture also allows for light management through microcavity effects when implemented in devices. We close by showcasing one benefit of this platform in IR CQD photodiodes: we achieve photon-to-electron conversion efficiencies of 70% at 1250 nm.[12]

Harvesting the IR solar spectrum beyond the cSi bandgap can provide an up to 15 mA·cm^{-2} short-circuit current, representing a potential addition of 7 absolute power points.[13] The transmittance of ITO decreases dramatically in this regime for a given sheet resistance (Figure 1a). The average infrared transmittance (AIRT) in the 1100−1800 nm window is limited to 32% when the sheet resistance is 10 Ω/□. Alternative TCEs such as OMO multilayers comprising thin metal films have been

explored to replace ITO in the visible; their performance and rational design have been little explored in the IR regime. In addition, even when high AIRT TCEs are used in CQD solar cells, IR light absorption is still low due to the low absorption coefficient of CQDs in the infrared (Figure 1b). Therefore, a newly designed TCE needs to provide a way to increase light absorption and, simultaneously, high AIRT and conductivity to achieve high-performance IR optoelectronics.

An ideal TCE for IR applications will maximize transparency in the IR without compromising electrical conductivity. We hypothesized that this could be achieved through an OMO multilayer structure composed of a series of layers:

- where a subset exhibited high IR transparency and low conductivity;

- where the remainder exhibited the needed high conductivity.

By designing such a structure so that the optical field was minimized in the higher-conductivity (less transparent) layers, we leverage the increased degrees of freedom available in a multilayer stack.

We began by estimating the optical transmittance of OMO structures using the transfer matrix formalism (TMF)[3,14,15] and compared it with that of thin metal films (Figure S1a). Silver (Ag) was selected as the metal in light of its lower parasitic absorption in the IR range compared to other metals such as Al, Au, and Cu.[4]

We used a constant refractive index of $n \approx 1.5$ and thickness of 30 nm for the oxide layer. In the case of bare Ag films, the transmittance rapidly decreases as the thickness of the Ag film increases, while its reflectance increases. Notably, the IR transmittance in the 1250−1600 nm region for Ag thin films is much lower than that in the visible light region (550 nm). OMO structures exhibit a high transmittance of over 90% at 550 nm, even at a metal thickness of 10 nm. (Figure S1a) Typical OMO structures can therefore ensure both high transmittance and low sheet resistance simultaneously in the visible regime because both oxide layers with a high refractive index reduce the reflection from the metal in the visible region.[16] In the IR range, however, OMO structures fail to provide significant benefits in transmittance even for metal films as thin as 6 nm. (Figure S1b)

We sought to break this limitation by incorporating asymmetry into the OMO multilayer stack and explored the refractive index (n) and thickness (t) parameter space of each oxide layer on both sides of the Ag film. The AIRT (1100−1800 nm) as a function of thickness (t_1, t_2) and refractive index (n_1, n_2) ratios of the two oxide layers (t_1, n_1: bottom; t_2, n_2: top) with fixed Ag film thickness (5 nm) is presented in Figure 2a. We fixed t_1 and n_1 to 30 nm and 1.5, respectively, and swept t_2 and n_2, finding that a higher AIRT is obtained as t_2/t_1 increases compared to a symmetric OMO. We observed two different regimes that can be classified depending on n_2/n_1. When $n_2/n_1 > 1$, a high AIRT is achieved when t_2/t_1 is in the 2−4 range and especially when the t_2/t_1 ratio is reduced as n_2/n_1 increases. When $n_2/n_1 < 1$, the overall AIRT gradually increases as t_2/t_1 increases. The AIRT increases as n_2/n_1 becomes smaller and is optimized for t_2/t_1 in the 5−7 range.

Figure S2 shows the calculated transmittance in the two identified regimes. The two regimes (2 and 3) exhibit different transmittance, but each has a higher AIRT compared to the standard regime 1. When sheet resistance is considered, regime 2 ($n_2/n_1 > 1$) provides a more realistic scenario without

excessively high t_2/t_1 ratios (the high t_2/t_1 ratio would require a thick top dielectric layer and thus a higher sheet resistance).

On the basis of these considerations, we designed an asymmetric OMO structure consisting of ITO/Ag/ZnO (IMZ) with the goal of high IR transmittance combined with low resistance (Figure 2b). We were able to limit ourselves to the use of a very thin (25 nm) layer of ITO; because ITO has a lower n value than other oxide materials in the IR, a higher n_2/n_1 ratio can be achieved (Figure S3). The value of 25 nm was also chosen to ensure a conformal layer with low roughness.

A chief requirement in the implementation of the IMZ structure is to achieve high quality and smooth metal and oxide films with precise control over their thickness. The growth of ultrathin metal films strongly depends on parameters such as substrate, evaporation conditions, and material surface energy. Polyethylenimine (PEI) has been reported to facilitate uniform metal nucleation.[17] We deposited a thin layer of PEI on top of ITO and then thermally evaporated a Ag layer. Atomic force microscopy (AFM) images reveal the uniform and smooth character of Ag films deposited on PEI as opposed to direct deposition on ITO (Figure 2b).

The top oxide layer was fabricated utilizing solution-processed ZnO nanoparticles, which combine an appropriate refractive index ($n \approx 1.9$) with an electron affinity that facilitates electron extraction in optoelectronic devices.[18,19] We confirmed that the addition of the top oxide layer dramatically enhanced the transmittance (Figure S4), which agrees with results in typical dielectric/metal/dielectric structures.[16]

We then sought to optimize experimentally the sheet resistance and transmittance of the IMZ TCE. We first monitored sheet resistance as a function of Ag film thickness (Figure 2c). For comparison, a symmetric ZnO(30 nm)/Ag(x nm)/ZnO(50 nm) (ZMZ) multilayer structure was characterized to verify the effect of ITO in the IMZ structure. In the case of a ZMZ structure, a sheet resistance of 100 Ω/□ at a Ag film thickness of 5 nm was obtained and gradually decreased to 10 Ω/□ as the Ag film thickness was increased to 7 nm. IMZs (without PEI), on the other hand, show a sheet resistance of 20− 30 Ω/□ for the same Ag thickness even though the Ag film is not uniform in this case (Figure 2b). This indicates that the ITO does play a role in lowering sheet resistance. The final structure of IMZ employing a PEI layer further reduced the resistance of the Ag film, resulting in ∼10 Ω/□ with a 5 nm thick Ag film.

The AIRT of the IMZ structures, presented as a function of Ag film thickness, is shown in Figure 2d. Typical ITO with 10 Ω/□ sheet resistance has an AIRT of approximately 32%, whereas the optimized IMZ multilayer showed an AIRT of 72%, a 2.3-fold increase at the same sheet resistance. The AIRT of the IMZ decreases as the Ag thickness increases due to the increased reflectivity of the Ag film. Remarkably, optimized IMZ electrodes exhibit a flat transmittance in the entire IR range from 1100 to 1800 nm, making them a compelling TCE for various IR optoelectronics.

Figure S5 shows a comparison of AIRT for various emerging transparent electrodes, including silver nanowire mesh,[10] carbon nanotubes (CNTs),[20,21] and multilayered graphene electrodes.[5] This comparison illustrates that the IMZ platform developed in this study exhibits improved optical and electrical characteristics compared to ITO in the IR region. In particular, the multilayer structure exhibits a notably lower resistance, crucial for applications such as light-emitting diodes and photovoltaics.[22]

To demonstrate the application of IMZs for IR optoelectronic applications and their potential for light management strategies
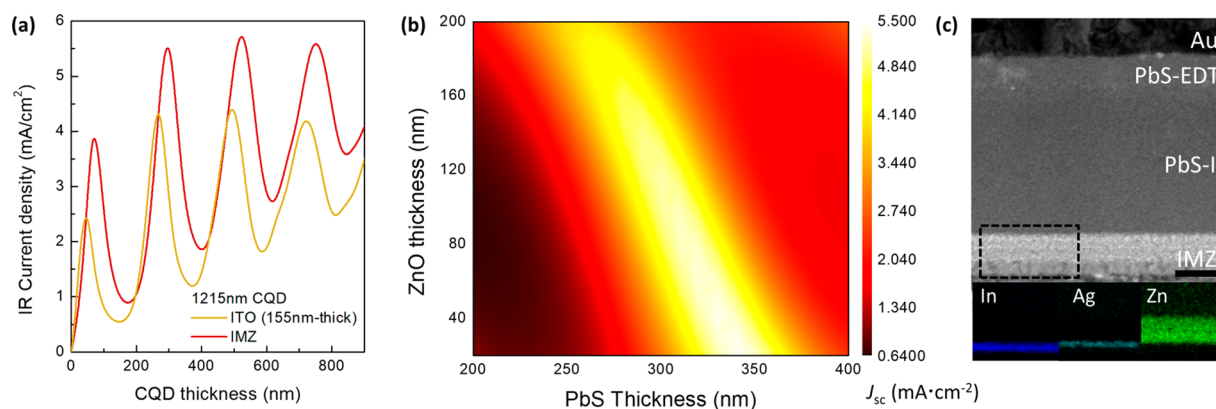
Figure 3. (a) IR current density of ITO- (yellow) and IMZ-based (red) PbS solar cells as a function of CQD layer thickness. IQE was assumed to be 100%, and incident solar irradiation was IR-filtered (<1100 cutoff). (b) Optimizing the IR microcavity effect as a function of ZnO and PbS thickness. (c) TEM cross-sectional image of IMZ-based IR CQDs solar cells. EDAX analysis of In (blue), Ag (dark green), and Zn (bright green) used to confirm the IMZ structure. Scale bar: 50 nm.
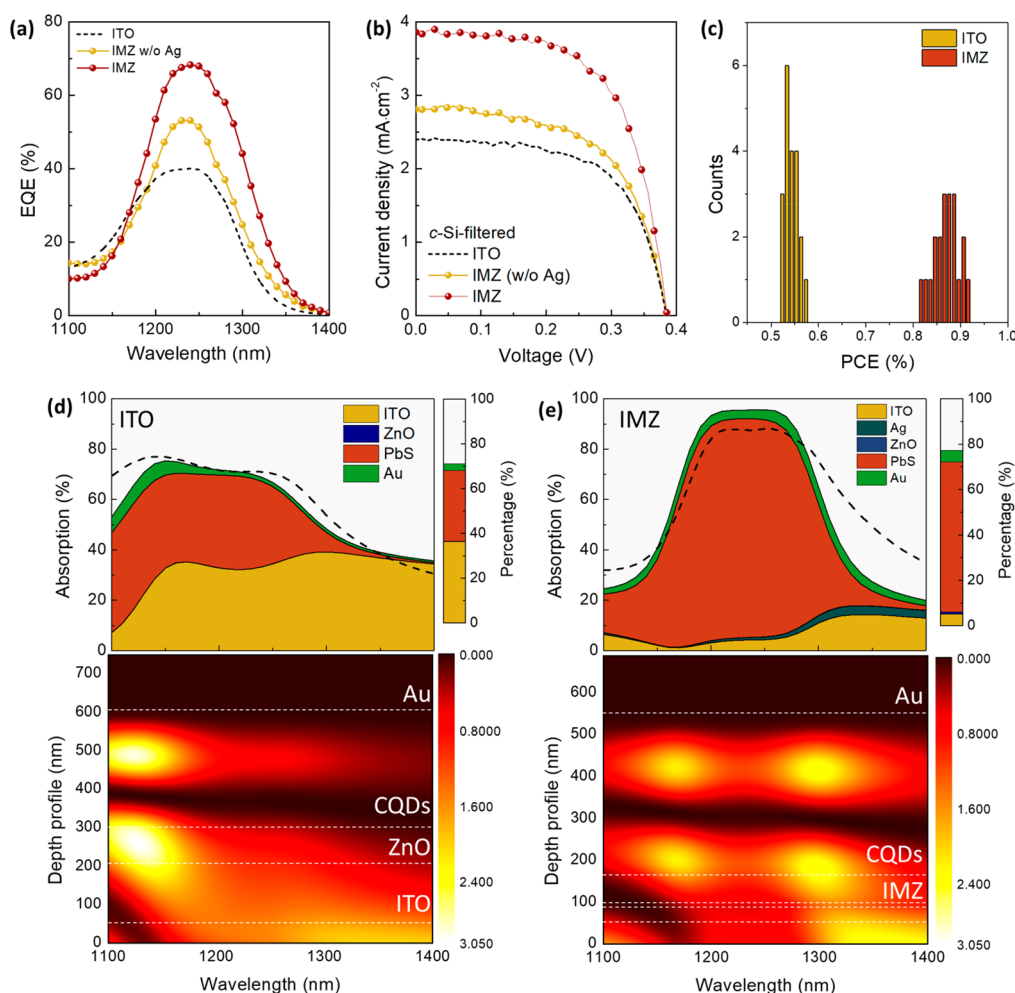

Figure 4. (a) EQE spectrum of ITO (black), IMZ (red), and IMZ without PEI+Ag (yellow). (b) *J−V* characteristics of CQD solar cells made with ITO (black), IMZ (red), and IMZ without PEI+Ag (yellow). (c) Statistical PCE histogram of ITO- (yellow) and IMZ-based (red) devices. (d) Calculated absorption in each layer and E-field distribution of thick ITO (~10 Ω/□, 155 nm)-based devices; ITO (yellow), PbS (red), ZnO (blue), Au (green), and reflection (gray). The complete structure is ITO(155 nm)/ZnO(80 nm)/CQDs(320 nm)/Au(120 nm). The dashed line denotes the measured total absorption. (e) Calculated absorption in each layer and E-field distribution of IMZ-based devices. The complete structure is ITO(25 nm):PEI(5 nm)/Ag(5 nm)/ZnO(80 nm)/CQDs(320 nm)/Au(120 nm). The dashed line denotes the measured total absorption.

in this regime, we fabricated IR-sensitive CQD solar cells with a 0.98 eV bandgap (Figure 3). OMO multilayers have been

reported to support microcavity modes when incorporated in thin films with a back reflecting mirror.[7,23] A cavity resonance

can be generated in IR CQD solar cells due to their high refractive index (∼3) and the possibility of depositing sufficiently thick layers (∼300 nm).[8] We sought therefore to investigate the IR microcavity effect in our IMZ platform for IR CQDs devices. A key parameter to provide efficient microcavity enhancement is resonance matching between two reflecting mirrors by controlling the ZnO and CQD layer thicknesses (Figure 3b). We observed Fabry−Perot interference effects that depend on the CQD layer thickness (Figure 3a). In order to generate constructive interference, it is important to match the optical length of the cavity with integer multiples of the wavelength of incident light.[24] As shown in Figure 3b, the cavity resonance depends strongly on the CQD layer thickness due to its larger refractive index ($n \approx 3$) compared to that of ZnO ($n \approx 1.9$). In the proposed CQD solar cell structure, we found that the microcavity resonance is maximized at a CQD layer thickness of approximately 300−350 nm. We found that higher current density is available with thinner ZnO layers for both conventional thick ITO (10 Ω/□) and IMZ devices (Figure S6).

On the basis of the above estimation, we built IR CQD devices utilizing our IMZ structure (see the Supporting Information). Transmission electron microscope (TEM) cross-sectional imaging reveals the device structure, which consists of IMZ(25 nm:5 nm/5 nm/80 nm)/PbS CQDs n-type layer(280 nm)/PbS CQDs p-type layer(40 nm)/Au. EDAX confirms the presence of the IMZ structure in the final device, with an ITO:PEI/Ag/ZnO stack (Figure 3c).

The external quantum efficiency (EQE) in the IR was then characterized (Figure 4a). To serve as control devices, thick ITO (∼10 Ω/□)-based CQD solar cells were also fabricated using the same ZnO and CQD thicknesses. The IMZ device shows a broad EQE enhancement compared to that of the ITO-based device in the overall wavelength range from 1170 to 1400 nm, with EQE values reaching 70% at the CQD exciton peak (1250 nm), compared to 40% in the case of the ITO-based device.

We then characterized the photovoltaic performance of the IR CQD solar cells under simulated AM1.5G illumination beyond the cSi bandgap (1100 nm) (Figure 4b). IMZ-based devices exhibited a higher short-circuit current (3.85 vs 2.40 mA·cm^{-2}) compared to the ITO-based controls, reaching a maximum IR-PCE of 0.96%, compared to 0.55% in the control samples (Table 1). A statistical histogram clearly depicts the PCE enhancement

Table 1. Photovoltaic Performance under Simulated cSi-Filtered AM1.5G Illumination

front electrode	V_{oc} (V)	J_{sc} (mA/cm^2)	FF (%)	IR-PCE (%)
IMZ	0.38	3.88	65.5	0.96
ITO (∼10 Ω/□)	0.37	2.40	62.4	0.55
IMZ (w/o PEI+Ag)	0.38	2.83	60.7	0.65

of IMZ devices (Figure 4c). These provided a 2-fold improvement in power conversion efficiency compared to previous microcavity IR CQD solar cells.[3]

To understand in greater depth the origins of the observed J_{sc} enhancement, we examined an additional condition with an IMZ structure excluding the metal and PEI film. Because such a structure was shown to have high AIRT reaching 90% (Figure 2d), a higher current density could reasonably be expected. However, the photocurrent did not show a notable enhancement compared to the control, low AIRT ITO (∼10 Ω/□) (Table 1). This result implies that the J_{sc} enhancement in the

IMZ device originates from a combination of higher AIRT and IR microcavity effects.

Figure 4d,e shows results of numerical modeling to estimate the predicted spectral absorption in the layer making up the IR CQD devices. In control devices (155 nm thick ITO), ITO absorbs 38% of the total incident photons, and the net absorption in the active layer is only about 30%. This is due to the IR electric field being mostly distributed near the ITO.

For IMZ devices, parasitic absorption is suppressed to below 10%, and the absorption in the CQD layer is significantly boosted to 60% as the E-field concentrates between Ag and Au electrodes. The measured total absorption matches well with TMF results, supporting the attribution of the enhancement to the IR microcavity effect.

In this study, we designed an IR multilayer structure with enhanced IR transmittance and low resistance for IR optoelectronic applications. The multilayer structure outperforms conventional ITO with 2.3-fold higher AIRT at the same sheet resistance. We found that IR CQD solar cells built on an IMZ electrode had nearly a 2-fold increased IR absorption compared to that of ITO control devices. This leads to an IR photoelectrical conversion efficiency of 70% at 1.25 μm and a record IR current density under Si-filtered simulated solar illumination. Optical modeling revealed that the origin of this absorption enhancement is a combination of IR microcavity effects between the IMZ and the Au back electrode and the improved AIRT.

In sum, we report herein enhanced IR CQD solar cells using microcavity effects. In addition, we proposed and studied a new transparent conductor platform—asymmetric multilayer electrodes—which we implemented to achieve high infrared transmittance (AIRT ≈ 72%) with low resistance (10 Ω/□). This new TCE platform can be incorporated in optoelectronic device applications also including light emission and sensing.

◼ EXPERIMENTAL SECTION

Solar Cell Characterization. The J−V characteristics of the solar cells were measured using a Keithley 2400 sourcemeter under a simulated AM1.5G solar spectrum (Sciencetech, class AAA) from a Xe lamp (Solar Light Company Inc.). The irradiation power was carefully calibrated with a reference Si solar cell at 100 mW·cm^{-2} (Newport, Inc.), and the aperture size of each device was 0.049 cm^2. The cSi filtering was simulated using an 1100 nm long-pass filter (Thorlabs). EQE spectra were measured under monochromatic illumination from a 400 W Xe lamp. For calibration, two photodetectors, a Newport 818-UV and Newport 838-IR, were used. The current response was collected at short-circuit conditions with a Lakeshore preamplifier connected to a Stanford Research 830 lock-in amplifier. The total absorption and transmittance were extracted from the reflection and via a UV−vis−IR spectrophotometer (Lambda 950). Cross-sectional imaging of the devices was obtained by focused ion beam (FIB, Helios 450 F1) and field-emission TEM (300 keV). The EDAX was performed simultaneously from the TEM results. AFM (BRUKER, multimode 8) was performed under scanasyst mode with a 1 Hz scanning speed. The sheet resistance was measured by a four-point probe (FPP5000, Veeco Inc.)

ASSOCIATED CONTENT

Ⓢ Supporting Information

The Supporting Information is available free of charge on the [ACS Publications website](#) at DOI: [10.1021/acsenergylett.8b01878](#).

> Experimental section, TMF calculation results, refractive index of each material, transmittance of IMZ electrode, figure of merit for AIRT vs the sheet resistance, and solar cell performance as a function of the ZnO thickness ([PDF](#))

AUTHOR INFORMATION

Corresponding Authors

*E-mail: jungyong.lee@kaist.ac.kr (J.-Y.L.).
*E-mail: ted.sargent@utoronto.ca (E.H.S.)

ORCID Ⓘ

Se-Woong Baek: 0000-0002-5197-0598
Olivier Ouellette: 0000-0001-5708-5058
Dae-Hyun Nam: 0000-0002-0871-1355
Li Na Quan: 0000-0001-9301-3764
Jung-Yong Lee: 0000-0002-5347-8230
Edward. H Sargent: 0000-0003-0396-6495

Notes

The authors declare no competing financial interest.

REFERENCES

(1) Garcia de Arquer, F. P.; Armin, A.; Meredith, P.; Sargent, E. H. Solution-Processed Semiconductors for Next-Generation Photodetectors. *Nat. Rev. Mater.* **2017**, *2*, 16100.

(2) Yuan, M. J.; Liu, M. X.; Sargent, E. H. Colloidal Quantum Dot Solids for Solution-Processed Solar Cells. *Nat. Energy* **2016**, *1*, 16016.

(3) Ouellette, O.; Hossain, N.; Sutherland, B. R.; Kiani, A.; García de Arquer, F. P.; Tan, H.; Chaker, M.; Hoogland, S.; Sargent, E. H. Optical Resonance Engineering for Infrared Colloidal Quantum Dot Photovoltaics. *ACS Energy Lett.* **2016**, *1*, 852−857.

(4) Ellmer, K. Past Achievements and Future Challenges in the Development of Optically Transparent Electrodes. *Nat. Photonics* **2012**, *6*, 809.

(5) Park, I. J.; Kim, T. I.; Yoon, T.; Kang, S.; Cho, H.; Cho, N. S.; Lee, J. I.; Kim, T. S.; Choi, S. Y. Flexible and Transparent Graphene Electrode Architecture with Selective Defect Decoration for Organic Light-Emitting Diodes. *Adv. Funct. Mater.* **2018**, *28*, 1704435.

(6) Sergeant, N. P.; Hadipour, A.; Niesen, B.; Cheyns, D.; Heremans, P.; Peumans, P.; Rand, B. P. Design of Transparent Anodes for Resonant Cavity Enhanced Light Harvesting in Organic Solar Cells. *Adv. Mater.* **2012**, *24*, 728−732.

(7) Liu, Q.; Romero-Gomez, P.; Mantilla-Perez, P.; Colodrero, S.; Toudert, J.; Martorell, J. A Two-Resonance Tapping Cavity for an Optimal Light Trapping in Thin-Film Solar Cells. *Adv. Energy Mater.* **2017**, *7*, 1700356.

(8) Zhang, X. L.; Johansson, E. M. J. Utilizing Light Trapping Interference Effects in Microcavity Structured Colloidal Quantum Dot Solar Cells: A Combined Theoretical and Experimental Approach. *Nano Energy* **2016**, *28*, 71−77.

(9) Siegmund, B.; et al. Organic Narrowband near-Infrared Photodetectors Based on Intermolecular Charge-Transfer Absorption. *Nat. Commun.* **2017**, *8*, 15421.

(10) Hu, L.; Kim, H. S.; Lee, J.-Y.; Peumans, P.; Cui, Y. Scalable Coating and Properties of Transparent, Flexible, Silver Nanowire Electrodes. *ACS Nano* **2010**, *4*, 2955−2963.

(11) Van De Groep, J.; Spinelli, P.; Polman, A. Transparent Conducting Silver Nanowire Networks. *Nano Lett.* **2012**, *12*, 3138−3144.

(12) Fan, J. Z.; et al. Halide Re-Shelled Quantum Dot Inks for Infrared Photovoltaics. *ACS Appl. Mater. Interfaces* **2017**, *9*, 37536−37541.

(13) Ip, A. H.; Kiani, A.; Kramer, I. J.; Voznyy, O.; Movahed, H. F.; Levina, L.; Adachi, M. M.; Hoogland, S.; Sargent, E. H. Infrared Colloidal Quantum Dot Photovoltaics Via Coupling Enhancement and Agglomeration Suppression. *ACS Nano* **2015**, *9*, 8833−8842.

(14) Peumans, P.; Yakimov, A.; Forrest, S. R. Small Molecular Weight Organic Thin-Film Photodetectors and Solar Cells. *J. Appl. Phys.* **2003**, *93*, 3693−3723.

(15) Pettersson, L. A.; Roman, L. S.; Inganäs, O. Modeling Photocurrent Action Spectra of Photovoltaic Devices Based on Organic Thin Films. *J. Appl. Phys.* **1999**, *86*, 487−496.

(16) Kim, S.; Lee, J.-L. Design of Dielectric/Metal/Dielectric Transparent Electrodes for Flexible Electronics. *J. Photonics Energy* **2012**, *2*, No. 021215.

(17) Kang, H.; Jung, S.; Jeong, S.; Kim, G.; Lee, K. Polymer-Metal Hybrid Transparent Electrodes for Flexible Electronics. *Nat. Commun.* **2015**, *6*, 6503.

(18) Kim, G. H.; Walker, B.; Kim, H. B.; Kim, J. Y.; Sargent, E. H.; Park, J.; Kim, J. Y. Inverted Colloidal Quantum Dot Solar Cells. *Adv. Mater.* **2014**, *26*, 3321−3327.

(19) Kyaw, A. K.; Wang, D. H.; Wynands, D.; Zhang, J.; Nguyen, T. Q.; Bazan, G. C.; Heeger, A. J. Improved Light Harvesting and Improved Efficiency by Insertion of an Optical Spacer (Zno) in Solution-Processed Small-Molecule Solar Cells. *Nano Lett.* **2013**, *13*, 3796−3801.

(20) Barnes, T. M.; Reese, M. O.; Bergeson, J. D.; Larsen, B. A.; Blackburn, J. L.; Beard, M. C.; Bult, J.; van de Lagemaat, J. Comparing the Fundamental Physics and Device Performance of Transparent, Conductive Nanostructured Networks with Conventional Transparent Conducting Oxides. *Adv. Energy Mater.* **2012**, *2*, 353−360.

(21) Hecht, D. S.; Hu, L. B.; Irvin, G. Emerging Transparent Electrodes Based on Thin Films of Carbon Nanotubes, Graphene, and Metallic Nanostructures. *Adv. Mater.* **2011**, *23*, 1482−1513.

(22) Morales-Masis, M.; De Wolf, S.; Woods-Robinson, R.; Ager, J. W.; Ballif, C. Transparent Electrodes for Efficient Optoelectronics. *Adv. Electron. Mater.* **2017**, *3*, 1600529.

(23) Sergeant, N. P.; Hadipour, A.; Niesen, B.; Cheyns, D.; Heremans, P.; Peumans, P.; Rand, B. P. Design of Transparent Anodes for Resonant Cavity Enhanced Light Harvesting in Organic Solar Cells. *Adv. Mater.* **2012**, *24*, 728−732.

(24) Agrawal, M.; Peumans, P. Broadband Optical Absorption Enhancement through Coherent Light Trapping in Thin-Film Photovoltaic Cells. *Opt. Express* **2008**, *16*, 5385−5396.